Defect modes in one-dimensional anisotropic photonic crystal

Noama Ouchani, Driss Bria, Bahram Djafari-Rouhani, Abdlekarim Nougaoui

Defect modes in one-dimensional anisotropic photonic crystal

Cite as: J. Appl. Phys. **106**, 113107 (2009); https://doi.org/10.1063/1.3266005
Submitted: 13 April 2009 • Accepted: 27 October 2009 • Published Online: 09 December 2009

N. Ouchani, D. Bria, B. Djafari-Rouhani, et al.

Defect modes in one-dimensional anisotropic photonic crystal

N. Ouchani,[1,a)] D. Bria,[1,2] B. Djafari-Rouhani,[2] and A. Nougaoui[1]
[1]*Département de Physique, Laboratoire de Dynamique et d'Optique des Matériaux, Faculté des Sciences, Université Mohamed Premier, 60000 Oujda, Morocco*
[2]*Institut d'Electronique, de Microélectronique et de Nanotechnologie (IEMN), UMR CNRS 8520, Universite de Lille 1, 59655 Villeneuve d'Ascq, France*

(Received 13 April 2009; accepted 27 October 2009; published online 9 December 2009)

We theoretically analyze the defect states in a single-defect photonic crystal composed of anisotropic dielectric materials. This structure can trap light of a given frequency range and filter only a certain frequency light. It is shown that the defect modes appear as peaks in the transmission spectrum. Their numbers, intensities, and frequency positions are extremely sensitive to the incidence angle and the orientation of the principal axes of layers constituting the superlattice and the layer defect. Our structure offers a great variety of possibilities for creating and controlling the number and transmitted intensities of defect modes. It can be a good candidate for realizing a selective electromagnetic filter. © *2009 American Institute of Physics*. [doi:10.1063/1.3266005]

I. INTRODUCTION

Photonic crystals (PCs) have attracted a fair amount of attention due to their ability of controlling the propagation of electromagnetic waves and the possibility of many potential applications in optoelectronic and optical communications.[1–6] A great deal of attention has been paid to periodically optical superlattice (SL) because of their outstanding optical properties. In particular, they offer novel efficient way of controlling the flow of light by exhibiting absolute photonic band gap, in which the propagation of optical wave is prohibited in all directions of space and for all polarization or by converting the polarization of optical incident wave ($S \Leftrightarrow P$), etc.

Applications of PCs can be enhanced by inserting a defect layer into a perfect PC structure. Properties of defect states are studied comprehensively in several works.[7–12] In Ref. 8 the authors studied the properties of the defect modes in one-dimensional (1D) PCs containing a defect layer with a negative index. They demonstrated that this kind of structure possesses many additional properties with respect to the conventional PCs. Ma *et al.*[10] presented the computational and experimental studies on a multimode defective 1D PC. This structure is constructed by introducing multiple defect layers into a 1D PC. It is shown that the separation of the neighboring defect modes can be monitored by modifying the structure parameters of the 1D PC. In Refs. 11 and 12 the authors investigated a defective structure consisting of alternating layers of liquid crystal and isotropic dielectrics. The director angle of liquid crystal layers can be controlled with an applied electric field. They studied that the defect mode frequency created by inserting a layer of liquid crystal into a 1D dielectric PC can be controlled by the application of an external voltage.

The objective of this paper is to theoretically investigate a single-defect PC that is composed of anisotropic dielectric materials. The birefringence of the layer is natural and the defect modes depend only on the parameters (thickness and orientation) of the birefringent defect layer. It is shown that the birefringence of layers has a significant effect on the number of defect modes inside the photonic band gap. We find that the behavior is, in general, more complex than that observed in defective 1D PC made of isotropic media.[13] We demonstrate that the number and the intensity of defect modes are extremely sensitive to the incidence angle and the orientation of the principal axes of the layers constituting the SL and the defect layer. The existence of spectral gaps and the defect properties of single-defective anisotropic PC are studied with a Green's function approach.

In anisotropic photonic structure, each incident plane wave with S or P polarization generates two reflected and two transmitted plane waves containing both S and P polarized plane waves. For special cases when the principal axes of the layers are parallel or perpendicular to fixed axes, the S and P polarized waves remain uncoupled.[6,14–17] Thus, a single incident $S(P)$ polarized plane wave produces a single reflected $S(P)$ polarized plane wave and a single transmitted $S(P)$ polarized plane wave. Our work is organized as follows: in Sec. II we present our theoretical expressions of the reflection and transmission coefficients when S or P polarized wave is incident upon the interface separating the substrate and the SL. Section III shows the numerical results when a defect layer is introduced in the middle of the perfect SL made of SbSI/$NaNO_2$ and embedded between two semi-infinite isotropic media (air). Finally, in Sec. IV, a summary is presented.

II. MODEL AND FORMALISM

The geometrical structure of single-defective anisotropic PC considered is schematically shown in Fig. 1. The defect layer labeled as 0 (material SbSI) is inserted at the center of the perfect PC structure. The unit cell of the structure is composed of two birefringent biaxial materials: $NaNO_2$ (material $i=1$) and SbSI (material $i=2$). All the structure is embedded between two isotropic media (air). The materials

[a)]Electronic mail: noama03@yahoo.fr.

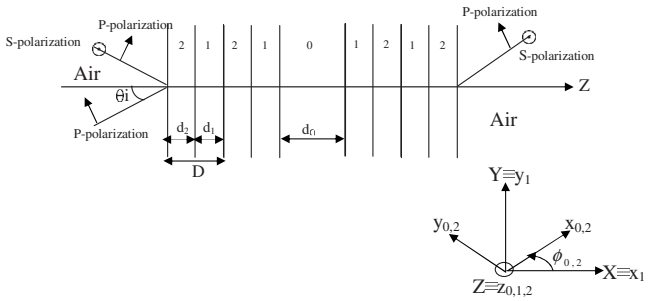

FIG. 1. Anisotropic multilayer structure formed by five layers of SbSI (material $i=2$) and four layers of $NaNO_2$ (material $i=1$). The defect layer SbSI of thickness d_0 is inserted in the middle of the SL, d_i $(i=0,1,2)$ is the thickness of layer i, D is the period of the finite system, and θ_i is the incident angle with respect to the Z axis. The crystal of the first layer has the principal axis directed along the direction of Cartesian axis, while the crystal axes of the second and defect layers are rotated with respect to the first one by the azimuth angle $\phi_{0,2}$ around the Z axis. The input and output isotropic medium is air and the incoming light has a P polarization.

constituting the layers $(i=0,1,2)$ of the structure are assumed homogeneous, nonmagnetic, and characterized by their thicknesses d_0, d_1, and d_2, respectively. The dielectric constants of material i in the principal axes (x,y,z) of the crystal are ϵ_x^i, ϵ_y^i, and ϵ_z^i. For a given orientation of each crystal, its dielectric tensor with respect to the fixed (XYZ) coordinate system is described by using the Euler angles[18,19] θ^i, ϕ^i, and ψ^i. For the sake of simplicity and without loss of generality, we investigate in our present study the effect of only the azimuth angle and omit the effect of the two other angles $(\theta=\psi=0)$. All the interfaces are taken to be parallel to the (XY) plane of a Cartesian (laboratory) coordinate system and the Z axis is along the normal to the interfaces. The number of the period at each side of defect is n. The period of the SL is $D=d_1+d_2$.

In the present paper, the study of the propagation of electromagnetic wave in periodic structure is performed with the help of the interface response theory of continuous media. The objective of this theory is to calculate the Green's function of a composite system containing a large number of interfaces that separate different homogeneous media. The knowledge of this Green's function enables us to obtain different physical properties of the system such as the reflection and transmission coefficients of the waves. In this theory, the Green's function of a composite system can be written as[20]

$$g(DD) = G(DD) + G(DM)\{[G(MM)]^{-1}g(MM)[G(MM)]^{-1} - [G(MM)]^{-1}\}G(MD), \quad (1)$$

where D and M are, respectively, the whole space and the space of the interfaces in the lamellar system. G is a block-diagonal matrix in which each block G_i correspond to the bulk Green's function of the subsystem i. All the matrix elements $g(DD)$ of the composite material can be obtained from the knowledge of the matrix elements $g(MM)$ of g in the interface space M.

The $g(MM)$ is calculated by inverting the matrix $g^{-1}(MM)$ formed out by a linear superposition of the surface matrix $g_s^{-1}(MM)$ of any independent film bounded by perfectly free interfaces with appropriate boundary conditions. The elements matrix $g_s^{-1}(MM)$ are given in the Appendix.

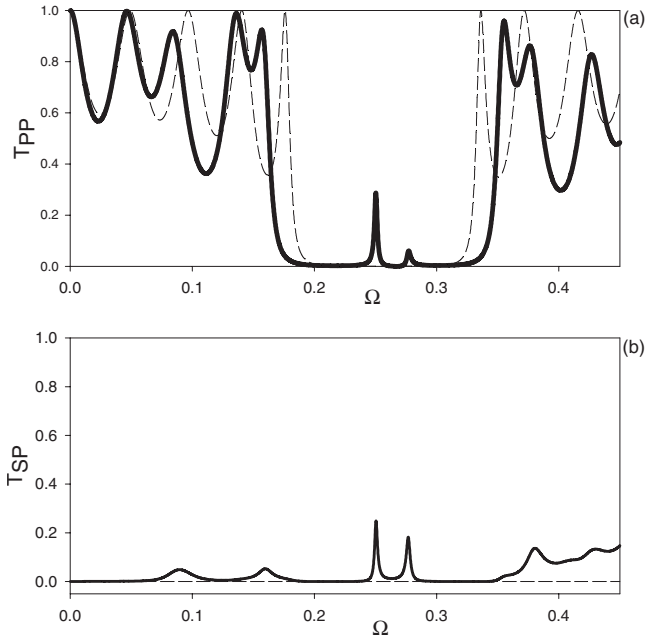

FIG. 2. Variation in the transmission coefficients T_{PP} (a) and T_{SP} (b) of the transmitted P and S polarized waves, respectively, as a function of the reduced frequency Ω. The dashed and solid lines correspond to the perfect and defective structures, respectively. The thickness of the defect layer is $d_0=0.65D$ and its orientation is characterized with the azimuthal angle $\phi_0=45°$. The layers constituting the perfect SL are characterized with $\phi_1=0°$, $\phi_2=0°$, and $n_z^{(1)}d_1=n_z^{(2)}d_2$. The incoming light has a P polarization.

Within this theory, the reflected and transmitted waves $u(D)$, resulting from a uniform plane wave $U(D)$ incident upon a plane boundary between two different media, are given by[20]

$$u(D) = U(D) + G(DM)\{[G(MM)]^{-1}g(MM)[G(MM)]^{-1} - [G(MM)]^{-1}\}U(M). \quad (2)$$

Let us mention that the incident wave, generated in the substrate S, can have two different polarizations, namely, S or P polarization. Each wave propagating inside the anisotropic media generates two transmitted waves and two reflected waves with different polarizations. Let us call E_{iS} and E_{iP} the amplitudes of the S and P components of the incident field. Then, the amplitudes of the reflected and transmitted fields can be written as[6]

$$\vec{E}_{RS}(z) = r_{SS}\vec{E}_{iS}(z) + r_{SP}\vec{E}_{iP}(z), \quad (3)$$

$$\vec{E}_{TS}(z) = t_{SS}\vec{E}_{iS}(z) + t_{SP}\vec{E}_{iP}(z), \quad (4)$$

$$\vec{E}_{RP}(z) = r_{PS}\vec{E}_{iS}(z) + r_{PP}\vec{E}_{iP}(z), \quad (5)$$

$$\vec{E}_{TP}(z) = t_{PS}\vec{E}_{iS}(z) + t_{PP}\vec{E}_{iP}(z). \quad (6)$$

The expressions of r_{ij} and t_{ij} in these equations, with $i,j=S$ or P, are given in the Appendix.

III. DISCUSSION AND NUMERICAL RESULTS

For the sake of simplicity, our perfect 1D anisotropic structure consists of alternating biaxial layers: five layers of SbSI (material $i=2$) and four layers of $NaNO_2$ (material i

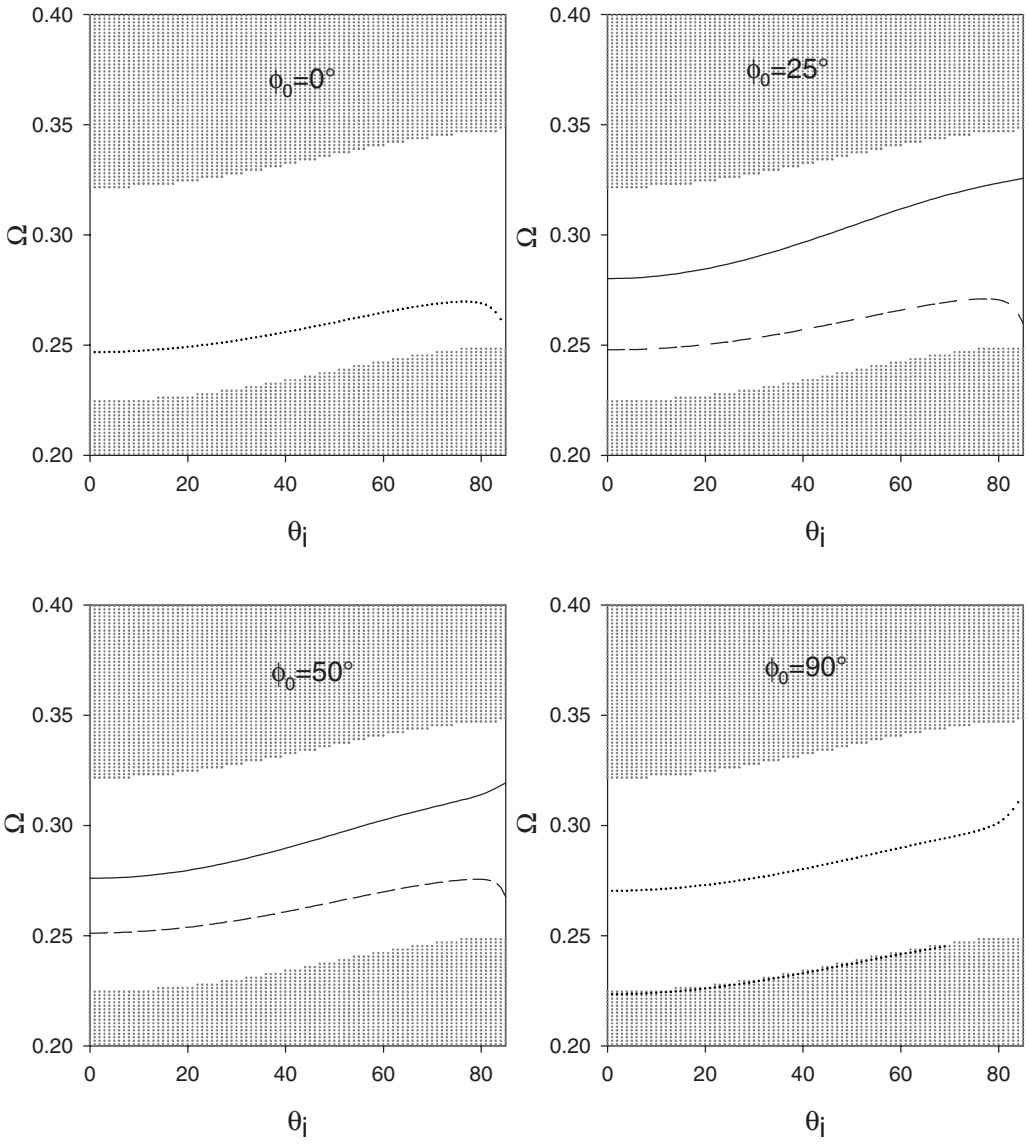

FIG. 3. Reduced frequency Ω of defect modes as a function of the incidence angle θ_i for several values of the azimuth angle ϕ_0 of defect layer, namely, $\phi_0=0°$, $\phi_0=25°$, $\phi_0=50°$, and $\phi_0=90°$. The other structural parameters are kept the same as in Fig. 2.

=1). The periodic structure is embedded between two isotropic media (air). This periodicity is broken by inserting a defect layer at the center of the pure PC structure, as depicted in Fig. 1. We assume that the defect layer is made of the SbSI material (similar to one type of layer in the perfect SL) with different thickness $d_0 \neq d_2$ and orientation ϕ_0. The principal optical indices of these materials are, respectively,[21] $n_x^{(1)}=1.344$, $n_y^{(1)}=1.411$, $n_z^{(1)}=1.651$ and $n_x^{(0,2)}=2.7$, $n_y^{(0,2)}=3.2$, $n_z^{(0,2)}=3.8$. The thicknesses d_1 and d_2 of the layers are chosen such that $n_z^{(1)}d_1=n_z^{(2)}d_2$ and the thickness of plane defect is $d_0=0.65D$, where D is the period of the SL. In most of our numerical results, we assume that the incoming light has a P polarization. After multiple reflection and transmission in the anisotropic media constituting the SL, the incoming wave produces two reflected (R_{SP} and R_{PP}) and two transmitted waves (T_{SP} and T_{PP}) with S and P polarizations, respectively. We display in Fig. 2 the transmission coefficients T_{PP} [Fig. 2(a)] and T_{SP} [Figs. 2(b)] versus the reduced frequency $\Omega=\omega D/2\pi c$ for a perfect PC (dashed lines) and a single-defect PC (solid lines). In this illustration, we suppose that the plane electromagnetic wave illuminates normally ($\theta_i=0$) the interface between the structure and the isotopic substrate. The principal axes of the materials constituting the perfect SL are chosen parallel to the fixed axes of the coordinate system (XYZ), i.e., $\phi_1=\phi_2=0°$, and we take $\phi_0=45°$ as the orientation of the defect layer. It is shown that two defect modes appear inside the lowest photonic band gap of the transmission spectrum for each polarization of the transmitted optical wave P [Fig. 2(a)] and S [Fig. 2(b)]. In the isotropic case, we can observe a single-defect mode, while in the anisotropic case this mode splits into two defect modes because in isotropic photonic structure, a single incident $S(P)$ polarized plane wave produces a single reflected $S(P)$ polarized plane wave and a single transmitted $S(P)$ polarized plane wave. However, in anisotropic photonic structure, each incident plane wave with S or P polarization generates two reflected and two transmitted plane waves containing both S and P polarized plane waves. These two propagating waves are coupled; thus, two modes appear in each transmission spectrum T_{PP} and T_{SP} at the same frequencies.

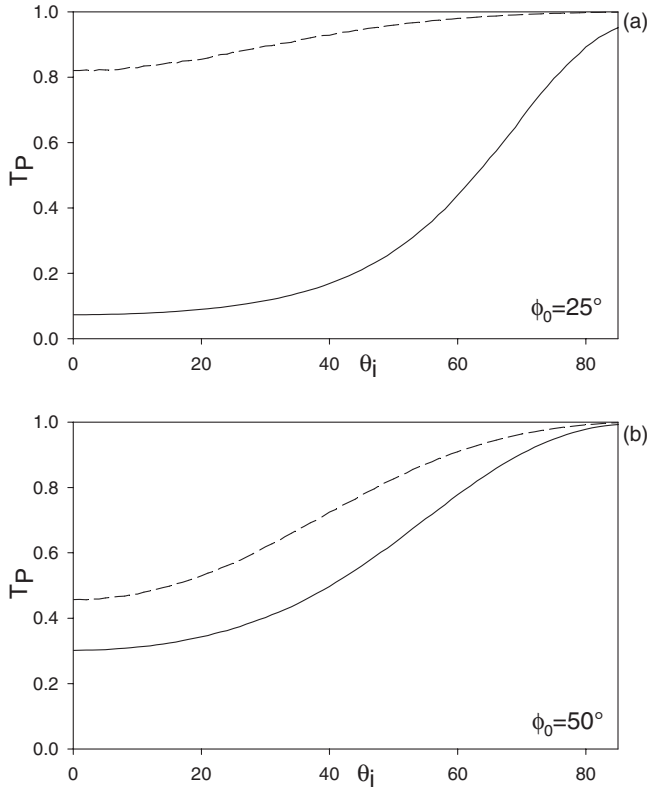

FIG. 4. Evolution of the transmission coefficient T_P vs the incidence angle θ_i for (a) ϕ_0=25° and (b) ϕ_0=50°. The other structural parameters are the same as in Fig. 2 and the incoming light has a P polarization.

Our defect layer is characterized with a thickness d_0 and an orientation ϕ_0 different from those of the SL layers. In the following, we investigate the existence and the number of defect states as function of the thickness and orientation of the defect layer. We present in Fig. 3 the dispersion curves (reduced frequency Ω) of the defect modes within the lowest band gap as function of the incident angle θ_i for different orientations of the defect layer SbSI: ϕ_0=0°, ϕ_0=25°, ϕ_0=50°, and ϕ_0=90°. The branches in this figure correspond to the maximum of the transmission coefficients T_P (T_P=T_{PP}+T_{SP}) when the incident light has a P polarization, while the gray areas represent the bulk bands of the infinite ideal SL. Note that the continuous bands in the infinite and semi-infinite SLs will break up into the discrete modes in the finite SL. Figure 3 shows a strong effect of the birefringence of defect layer on the number of defect states inside the band gap. When the principal axes of defect layer are parallel (ϕ_0=0°) or perpendiculaire (ϕ_0=90°), one branch appears within the band gap. An incident polarized plane wave (P) produces a single transmitted polarized plane wave P with a transmission coefficient T_{PP} (T_{SP}=0). The situation is then similar to the one corresponding to the case of isotropic system. For other orientations of the principal axes of layer defect, ϕ_0=25°; ϕ_0=50°, a single incident plane wave (P) produces two transmitted plane waves containing both S and P polarized plane waves, with the transmission coefficients T_{SP} and T_{PP}, respectively. Thus, two defect modes are cerated inside the band gap at two different frequencies.

However, the intensities of the defect states change significantly versus the incident angle θ_i, as represented in Fig. 4. It is shown that the profile for ϕ_0=25° [Fig. 4(a)] is different from that for ϕ_0=50° shown in Fig. 4(b). For both cases, the intensities T_P of the defect modes gradually increase when the incoming light is very obliquely incident into the structure. To understand in more detail the behavior

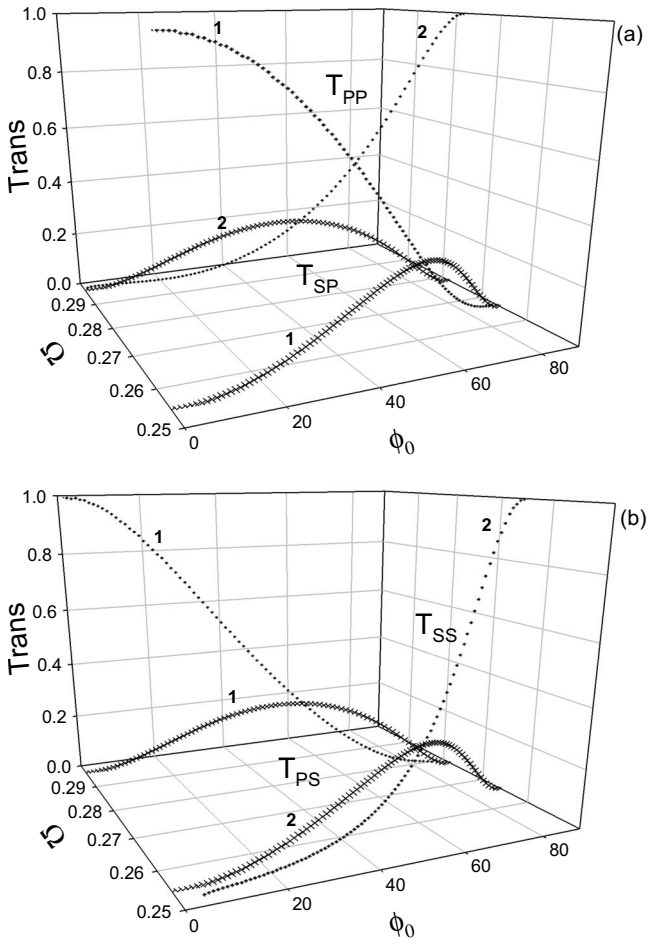

FIG. 5. Variation in the transmitted intensities of the polarized waves as a function of both the reduced frequency and the azimuthal angle ϕ_0 of defect layer SbSI when the input light has a (a) P or (b) S polarization. The dotted line corresponds to T_{PP} or T_{SS} and the crossed line corresponds to T_{SP} or T_{PS}. The incoming light has a P polarization with an incidence angle θ_i =35°.

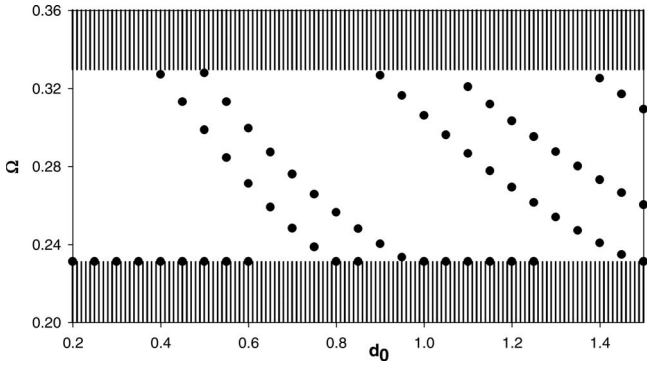

FIG. 6. Dependence of number and frequency of defect modes with the thickness d_0 of defect layer. The azimuthal angle of defect layer is ϕ_0 =50° and the azimuthal angles of the layers constituting the perfect SL are ϕ_1=0°, ϕ_2=0°. The incoming light has a P polarization with an incidence angle θ_i=35°.

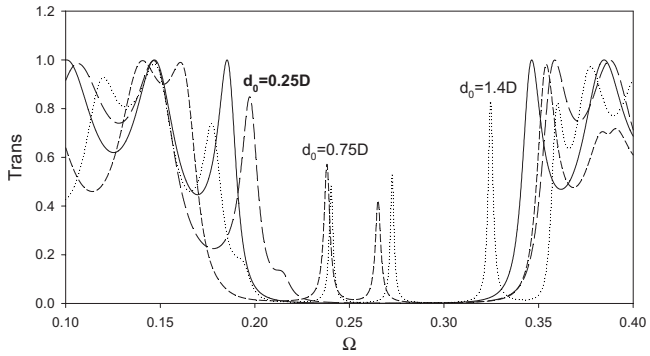

FIG. 7. Transmission spectra through perfect structure (solid line) and defective PC (dashed line) with different thicknesses d_0 of the defect layer. The others parameters are the same as Fig. 6.

of transmission coefficient, we have plotted in Figs. 5(a) and 5(b), the evolution of the transmission coefficients as a function of both the reduced frequency and the azimuthal angle ϕ_0 of defect layer, when the input light has a P [Fig. 5(a)] or S [Fig. 5(b)] polarization with an incidence angle $\theta_i=35°$. Inside the first band gap, the position and the form of these branches change significantly versus the orientation of the biaxial defect layer. The intensities T_{SP} and T_{PS} of the two defect modes (1 and 2) vary in the same way, they are important in the region when the two transmitted waves are coupled, and tend toward zero when the waves S and P become decoupled, around 0° and 90°. On the other hand, the intensities T_{PP} and T_{SS} of these modes (1 and 2) have an opposite behavior when the orientation of azimuthal angle changes from 0° to 90°. This opposite variation in the intensities T_{PP} and T_{SS} of the two defect modes is due to the coupling between S- and P-polarized waves. Each mode has a polarization different to the other mode.

In all the above illustrations, we have studied only the effect of the azimuthal angle ϕ_0 of defect layer without changing its thickness d_0. In order to evaluate the effect of this parameter, we present in Fig. 6 the evolution of the number of defect modes as function of d_0 inside the first band gap, for an arbitrary value of azimuthal angle ϕ_0. It is shown that the number of states depends slightly on the thickness d_0 of defect layer. For some values of thickness d_0, we have illustrated in Fig. 7, the evolution of the transmission intensities as function of reduced frequency Ω. One can

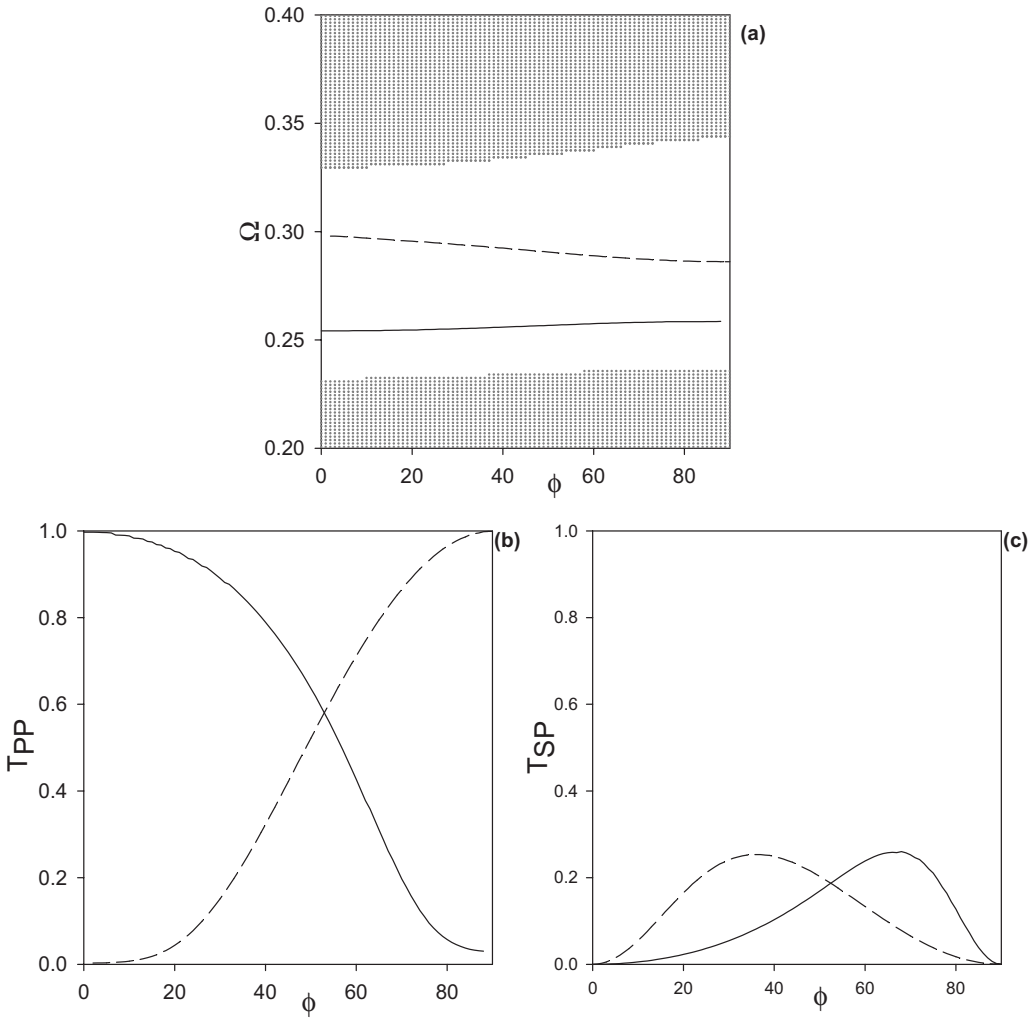

FIG. 8. Reduced frequency Ω of the defect modes (a) and transmitted intensities T_{PP} and T_{SP} [(b) and (c)] vs the azimuthal angle ϕ ($\phi=\phi_0=\phi_2$). The gray area correspond to the bulk bands of the infinite SL. The other parameters are kept the same as in Fig. 2 and the incoming light has a P polarization with an incidence angle $\theta_i=35°$.

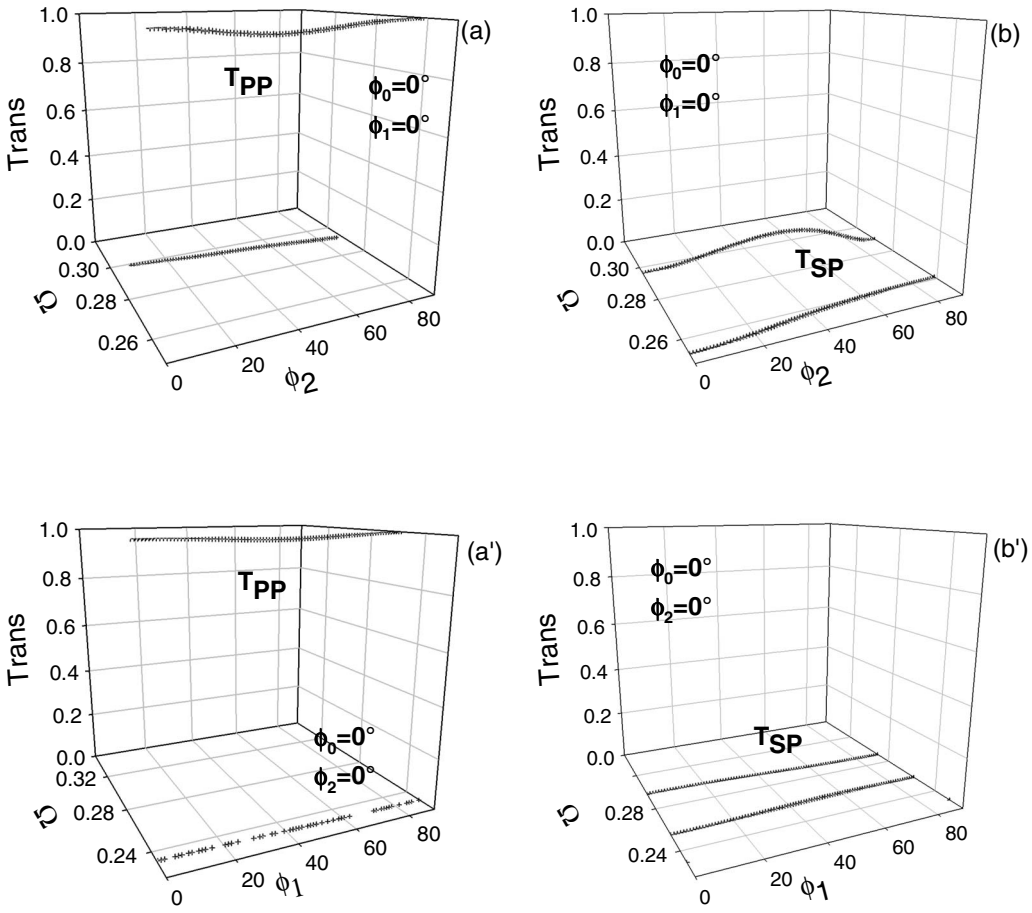

FIG. 9. Variation in the transmitted intensities of P polarized wave (T_{PP}) and S polarized wave (T_{SP}) as a function of both the reduced frequency and the azimuthal angle ϕ_2 of SbSI layers constituting the SL [(a) and (b)], while keeping $\phi_0=\phi_1=0°$, and ϕ_1 of the $NaNO_2$ layers constituting the SL [(a′) and (b′)], while keeping $\phi_0=\phi_2=0°$. The input light has a P polarization with an incidence angle $\theta_i=35°$.

notice that these defect modes appear at different frequency inside the lowest band gap.

Let us now analyze the effect of the orientations of the layers constituting the perfect SL. First, we suppose that $\phi_1=0°$ in the $NaNO_2$ layers and we change the orientation of all the SbSI layers including the defect layer ($\phi_2=\phi_0$) in order to show the influence of this parameter on the results. Figure 8(a) shows the dispersion curves of defect states within the lowest band gap as a function of the azimuth angle ϕ (with $\phi=\phi_0=\phi_2$) of all the SbSI layers. Two modes appear inside this band gap with different frequencies. The intensities of defect modes are strongly dependent on the orientation of the principal axes of the layers SbSI in the SL as depicted in curves [Figs. 8(b) and 8(c)]. The intensity of the first defect mode T_{PP} (solid line) has an opposite behavior than the second defect mode (dashed line). In curves Figs. 8(b) and 8(c), one can remark that the number of defect modes in the transmission spectrum depends on the coupling between S- and P-polarized modes: two modes appear in the region when the coupling of S and P is very strong and one mode where S and P are uncoupled. These results are similar to those observed in Fig. 5, while keeping $\phi_2=0$ and modulating the orientation of the defect layer.

In a second study, we chose the azimuthal angle of the defect layer $\phi_0=0°$ and we change independently the orientations of the SbSI layers [Figs. 9(a) and 9(b)] and of the $NaNO_2$ layers [Figs. 9(a) and 9(b)]. It appears clearly that the behaviors of defect modes are completely different than the results obtained when the defect layer has an arbitrary orientation. Only one mode has a significant intensity almost equal to 1, with the same polarization as the incident wave. This single mode within the lowest band gap is due to isotropy ($\phi_0=0$) of the defect layer.

The change in the orientation of the birefringent defect layer offers a great variety of possibilities for creating and controlling the number of defect modes as well as the defect mode frequencies and mode intensities.

IV. CONCLUSIONS

In conclusion, it has been analyzed in this work that a single-defective anisotropic PC can be exploited in the fabrication of an optical filter. We progressively demonstrated the effect of different parameters of defect layer and the layers constituting the perfect SL. It appears clearly that the change in the orientation of the birefringent defect layer offers a great variety of possibilities for creating and controlling the number of defect modes as well as the defect mode frequencies and intensities.

ACKNOWLEDGMENTS

D.B. acknowledges the hospitality of the *Institut d'Electronique, de Microélectronique et de Nanotechnologie (IEMN)*, Université de Lille 1 (France) where part of this work has been done.

APPENDIX: RESPONSE FUNCTIONS, TRANSMITTED AND REFLECTED COEFFICIENTS OF ANISOTROPIC PHOTONIC CRYSTAL

(1). The bulk Green's function elements are given by

$$G_{XX}(Z,Z') = -\frac{C}{2\alpha_-\alpha_+}[\alpha_- A_- \exp(-\alpha_+|Z-Z'|) - \alpha_+ A_+ \exp(-\alpha_-|Z-Z'|)],$$

$$G_{YX}(Z,Z') = -\frac{B}{D}\frac{C}{2\alpha_-\alpha_+}[\alpha_- \exp(-\alpha_+|Z-Z'|) - \alpha_+ \exp(-\alpha_-|Z-Z'|)],$$

$$G_{ZX}(Z,Z') = -\frac{iq_Y C}{2}\frac{\epsilon_{XY}}{\epsilon_{ZZ}}[\exp(-\alpha_+|Z-Z'|) - \exp(-\alpha_-|Z-Z'|)]\mathrm{sgn}(Z-Z'),$$

$$G_{XY}(Z,Z') = -\frac{B}{D}\frac{C}{2\alpha_-\alpha_+}[\alpha_- \exp(-\alpha_+|Z-Z'|) - \alpha_+ \exp(-\alpha_-|Z-Z'|)],$$

$$G_{YY}(Z,Z') = -\frac{C}{2\alpha_-\alpha_+ D}[\alpha_- A_+ \exp(-\alpha_+|Z-Z'|) - \alpha_+ A_- \exp(-\alpha_-|Z-Z'|)],$$

$$G_{ZY}(Z,Z') = -\frac{C}{2}\frac{iq_Y}{q_0^2\epsilon_{ZZ}}[A_+ \exp(-\alpha_+|Z-Z'|) - A_- \exp(-\alpha_-|Z-Z'|)]\mathrm{sgn}(Z-Z'),$$

$$G_{XZ}(Z,Z') = -\frac{iq_Y C}{2}\frac{\epsilon_{XY}}{\epsilon_{ZZ}}[\exp(-\alpha_+|Z-Z'|) - \exp(-\alpha_-|Z-Z'|)]\mathrm{sgn}(Z-Z'),$$

$$G_{YZ}(Z,Z') = -\frac{C}{2}\frac{iq_Y}{q_0^2\epsilon_{ZZ}}[A_+ \exp(-\alpha_+|Z-Z'|) - A_- \exp(-\alpha_-|Z-Z'|)]\mathrm{sgn}(Z-Z'),$$

$$G_{ZZ}(Z,Z') = \frac{1}{q_Y^2 - q_0^2\epsilon_{ZZ}}\left\{\frac{1}{D}\delta(Z-Z') + \frac{C}{2}\frac{q_Y^2}{q_0^2\epsilon_{ZZ}}[\alpha_+ A_+ \exp(-\alpha_+|Z-Z'|) - \alpha_- A_- \exp(-\alpha|Z-Z'|)]\right\}, \quad \text{(A1)}$$

where $A_\pm = (q_Y^2 - q_0^2\epsilon_{XX} - \alpha_\pm^2)$, $B = q_0^2\epsilon_{XY}$, $C = (\alpha_+^2 - \alpha_-^2)^{-1}$, $D = q_0^2\epsilon_{ZZ}(q_Y^2 - q_0^2\epsilon_{ZZ})^{-1}$, and $\delta(Z-Z')$ the dirac delta function.

$q_0 = \omega/c$ is the vacuum wave vector, c is the velocity of light in vacuum, and ω is the frequency of optical wave.

ϵ is the dielectric tensor defined in the laboratory system (XYZ), with $\theta=0$, $\psi=0$, and an arbitrary value of azimuth angle ϕ, by

$$\epsilon = \begin{pmatrix} \epsilon_x\cos^2(\phi) + \epsilon_y\sin^2(\phi) & (\epsilon_x - \epsilon_y)\cos(\phi)\sin(\phi) & 0 \\ (\epsilon_x - \epsilon_y)\cos(\phi)\sin(\phi) & \epsilon_x\sin^2(\phi) + \epsilon_y\cos^2(\phi) & 0 \\ 0 & 0 & \epsilon_x \end{pmatrix}, \quad \text{(A2)}$$

$\alpha_\pm$ are defined as

$$-q_Z^2 = \alpha_\pm^2, \quad \text{(A3)}$$

$$\alpha_\pm^2 = \frac{1}{2\epsilon_{ZZ}}([q_Y^2(\epsilon_{ZZ}+\epsilon_{YY}) - q_0^2\epsilon_{ZZ}(\epsilon_{XX}+\epsilon_{YY})] \pm \{[k_Z^2\epsilon_{YY} - \epsilon_{ZZ}(q_Y^2 - q_0^2\epsilon_{XX})]^2 - 4q_0^2k_Z^2\epsilon_{ZZ}\epsilon_{XY}^2\}^{1/2}), \quad \text{(A4)}$$

where $k_Z^2 = q_Y^2 - q_0^2\epsilon_{ZZ}$.

(2). The surface response function of finite layer of a homogenous medium i, extending in the region $-d_0/2 \leqslant Z \leqslant d_0/2$ with free surfaces, is given by

$$[g_i(MM)]^{-1} = \begin{pmatrix} A_i & B_i \\ B_i & A_i \end{pmatrix} \quad \text{(A5)}$$

where A_i and B_i are 2×2 matrices, whose elements are the forms

$$A_i = \begin{pmatrix} r_i & q_i \\ q_i & k_i \end{pmatrix} \quad \text{and} \quad B_i = \begin{pmatrix} h_i & f_i \\ f_i & e_i \end{pmatrix}, \quad \text{(A6)}$$

where r_i, q_i, k_i, h_i, f_i, and e_i are defined as

$$r_i = -C_i[\alpha_{i+}A_{i-}\coth\theta_{i+} - \alpha_{i-}A_{i+}\coth\theta_{i-}],$$

$$q_i = C_iB_i[\alpha_{i+}\coth\theta_{i+} - \alpha_{i-}\coth\theta_{i-}],$$

$$k_i = -C_iD_i[\alpha_{i+}A_{i+}\coth\theta_{i+} - \alpha_{i-}A_{i-}\coth\theta_{i-}],$$

$$h_i = C_i[\alpha_{i+}A_{i-}(\sinh\theta_{i+})^{-1} - \alpha_{i-}A_{i+}(\sinh\theta_{i-})^{-1}],$$

$$f_i = C_iB_i[\alpha_{i-}(\sinh\theta_{i-})^{-1} - \alpha_{i+}(\sinh\theta_{i+})^{-1}],$$

$$e_i = -C_iD_i[\alpha_{i-}A_{i-}(\sinh\theta_{i-})^{-1} - \alpha_{i+}A_{i+}(\sinh\theta_{i+})^{-1}], \quad \text{(A7)}$$

with $A_{i\pm} = (q_Y^2 - q_0^2\epsilon_{XX}^{(i)} - \alpha_{i\pm}^2)$, $B_i = q_0^2\epsilon_{XY}^{(i)}$, $C_i = (\alpha_{i+}^2 - \alpha_{i-}^2)^{-1}$, $D_i = q_0^2\epsilon_{ZZ}^{(i)}(q_Y^2 - q_0^2\epsilon_{ZZ}^{(i)})^{-1}$ and $\theta_{i\pm} = \alpha_{i\pm}d_i$.

(3). The expressions of the amplitude transmitted (t_{SS}, t_{PS}) and reflected (r_{SS}, r_{PS}) coefficients, when a pure (S) wave is incident, are the form

$$r_{SS} = -(2\alpha d_{11} + 1),$$

$$r_{PS} = -(2\alpha d_{21})\frac{B_s}{B_p},$$

$$t_{SS} = -(2\alpha d_{13}),$$

$$t_{PS} = -(2\alpha d_{23})\frac{B_s}{B_p}, \tag{A8}$$

where $\alpha=(k_{\parallel}^2-\omega^2\epsilon_s/c^2)^{1/2}$ with $k_{\parallel}$ as the wave vector parallel to the (XY) interfaces, ω is the frequency of optical wave, c is the speed of light in vacuum, and ϵ_s is the permittivity of substrate.

$B_s=1$ is the amplitude of the S wave and B_p ($B_p=-i\alpha c/\omega\sqrt{\epsilon_s}$) is the amplitude of the P input wave.

d_{11}, d_{21}, d_{13}, and d_{23} are the elements of tranked matrix of the finite system inserted between the two substrates, presented in Fig. 1.

(4). The expressions of the amplitude transmitted (t_{PP},t_{SP}) and reflected (r_{PP},r_{SP}) coefficients, when a pure P waves is incident, are of the form

$$r_{PP} = \left(\frac{2q_0^2\epsilon_s}{\alpha}d_{22} - 1\right),$$

$$r_{SP} = \left(\frac{2q_0^2\epsilon_s}{\alpha}d_{12}\right)\frac{B_p}{B_s},$$

$$t_{SP} = \left(\frac{2q_0^2\epsilon_s}{\alpha}d_{14}\right)\frac{B_p}{B_s},$$

$$t_{PP} = \left(\frac{2q_0^2\epsilon_s}{\alpha}d_{24}\right) \tag{A9}$$

as the same d_{12}, d_{22}, d_{14}, and d_{24} are the elements of tranked matrix of the finite system.

We note here that the total reflectivities for the P and S modes are

$$R_P \equiv R_{PP} + R_{SP} = |r_{PP}|^2 + |r_{SP}|^2, \tag{A10}$$

$$R_S \equiv R_{SS} + R_{PS} = |r_{SS}|^2 + |r_{PS}|^2, \tag{A11}$$

and the total transmission for the P and S modes have the following expressions:

$$T_P \equiv T_{PP} + T_{SP} = |t_{PP}|^2 + |t_{SP}|^2, \tag{A12}$$

$$T_S \equiv T_{SS} + T_{PS} = |t_{SS}|^2 + |t_{PS}|^2, \tag{A13}$$

[1] E. Yablonovitch, Phys. Rev. Lett. **58**, 2059 (1987).
[2] D. Bria, B. Djafari-Rouhani, E. H. El Boudouti, A. Mir, A. Akjouj, and A. Nougaoui, J. Appl. Phys. **91**, 2569 (2002).
[3] D. Bria, B. Djafari-Rouhani, A. Akjouj, L. Dobrzynski, J. P. Vigneron, E. H. El Boudouti, and A. Nougaoui, Phys. Rev. E **69**, 066613 (2004).
[4] H. Y. Lee, H. Makino, T. Yaoand, and A. Tanaka, Appl. Phys. Lett. **81**, 4502 (2002).
[5] L. M. Zhao and B.-Y. Gu, Appl. Phys. Lett. **88**, 122904 (2006).
[6] N. Ouchani, D. Bria, B. Djafari-Rouhani, and A. Nougaoui, J. Opt. Soc. Am. A **24**, 2710 (2007).
[7] H. Nemec, L. Duvillaret, F. Quemeneur, and P. Kuzel, J. Opt. Soc. Am. B **21**, 3 (2004).
[8] K.-Y. Xu, X. Zheng, and W.-L. She, Appl. Phys. Lett. **85**, 25 (2004).
[9] H. Nemec, P. Kuzel, F. Garet, and L. Duvillaret, Appl. Opt. **43**, 1965 (2004).
[10] G. Ma, J. Shen, Z. Zhang, Z. Hua, and S. H. Tang, Opt. Express **14**, 2 (2006).
[11] Y.-K. Ha, Y.-C. Yang, J.-E. Kim, H. Y. Parka, C.-S. Kee, H. Lim, and J.-C. Lee, Appl. Phys. Lett. **79**, 15 (2001).
[12] J. Cos, J. Ferre-Borrull, J. Pallares, and L. F. Marsal, Opt. Commun. **282**, 1220 (2009).
[13] A. Mir, A. Akjouj, E. H. El Boudouti, B. Djafari-Rouhani, and L. Dobrzynski, Vacuum **63**, 197 (2001).
[14] N. Ouchani, D. Bria, A. Nougaoui, and B. Djafari-Rouhani, Sol. Cells **90**, 1445 (2006).
[15] P. Yeh, J. Opt. Soc. Am. **69**, 742 (1979).
[16] A. Mandatori, C. Sibilia, M. Centini, G. DAguanno, M. Bertolotti, M. Scalora, M. Bloemer, and C. Bowden, J. Opt. Soc. Am. B **20**, 504513 (2003).
[17] C. Vandenbem, J. Vigneron, and J. Vigoureux, J. Opt. Soc. Am. B **23**, 2366 (2006).
[18] H. Goldstein, *Classical Mechanics* (Addison-Wesley, Reading, MA, 1957), Chap. 4, pp. 107–109.
[19] G. D. Landry and T. A. Maldonado, J. Opt. Soc. Am. A **12**, 2048 (1995).
[20] L. Dobrzynski, Surf. Sci. **180**, 489 (1987); Surf. Sci. Rep. **11**, 139 (1990); L. Dobrzynski and H. Puszkarski, J. Phys.: Condens. Matter **5**, 139 (1993).
[21] P. Yeh, *Optical Waves in Layered Media* (Wiley, New York, 1988), Chap. 9.